Towards high performance Cd-free CZTSe solar cells with ZnS(O,OH) buffer layer: The influence of the thiourea concentration in the chemical bath deposition

Markus Neuschitzer[1], Karla Lienau[2], Maxim Guc[1], Lorenzo Calvo Barrio[3], Stefan Haass[2], Jose Marquez Prieto[4], Yudania Sanchez[1], Moises Espindola-Rodriguez[1], Yaroslav Romanyuk[2], Alejandro Perez-Rodriguez[1,5], Victor Izquierdo-Roca[1], and Edgardo Saucedo[1]

[1] Catalonia Institute for Energy Research- IREC, Jadins de les Dones de Negre 1, 08930 Sant Adrià de Besòs (Barcelona), Spain
[2] Empa – Swiss Federal Laboratories for Materials Science and Technology, Laboratory for Thin Films and Photovoltaics, 8600 Dübendorf, Switzerland
[3]Centres Científics i Tecnològics CCiTUB, Universitat de Barcelona, C. Lluis Solé i Sabarés 1, 08028 Barcelona, Spain
[4] Northumbria Photovoltaic Applications Group, Department of Physics and Electrical Engineering, Northumbria University, Newcastle upon Tyne NE1 8ST
[5] IN2UB, Departament d'Electrònica, Universitat de Barcelona, C. Martí i Franquès 1, 08028 Barcelona, Spain

ABSTRACT

High performance kesterite (CZTSe) based solar cell devices usually employ an absorber/buffer heterostructure using toxic CdS deposited by chemical bath deposition (CBD) as buffer layer. This is due to the favourable spike like conduction band alignment of CdS buffer and CZTSe absorber. ZnS(O,OH) buffer layers provide a promising nontoxic alternative. Here, a variation of the thiourea concentration in the CBD of ZnS(O,OH) buffer layers and its influence on device performances of pure selenide kesterite heterostructure solar cells is presented. Furthermore, the influence of buffer layer deposition conditions on light induces metastabilities are discussed. ZnS(O,OH) buffer deposited with high thiourea concentration leads to distorted illuminated JV curves as expected for devices with unfavourable high spike like conduction band alignment between buffer and CZTSe absorber. By adjusting the thiourea concentration JV curve distortions can be reduced. An optimized CBD process leads to device efficiency of up to 6.5% after light soaking which is comparable to the efficiency of a reference device employing CdS as buffer layer (6.9%).

Keywords: thin film solar cell, buffer layer, chalcogenides, CZTSe, Cd-free, ZnS(O,OH), light soaking

1.Introduction

In recent years kesterite $Cu_2ZnSn(S_{1-x}Se_x)_4$ (CZTSSe) attracted much attention as possible alternative to more mature chalcopyrites ($CuIn_{1-x}Ga_xSe_2$ – CIGS) p-type absorber material for thin film solar cells due to its composition of more abundant elements.[1] Different to most silicon solar cells where a homojunction is created by doping of the Si, chalcogenide thin film solar cells use a heterojunction architecture to create the p-n junction for the separation of light generated electron hole pairs.[2] This heterostructure consist of a polycrystalline

semiconducting absorber material and some kind of transparent emitter, completed with front and back contacts. In a heterostructure, the electric properties of the junction strongly depend on the energy band alignment at the interface of the two different semiconducting materials. Kesterite based solar cell devices employ a p-type absorber/ n-type buffer/window heterostructure to form the p-n junction.[1] The role of the buffer layer is to provide an optimal conduction band alignment of absorber/buffer/window heterostructure which is crucial for high device performance and a so called spike like band alignment is favourable.[2,3] In a spike like alignment the conduction band minimum of the n-type buffer layer has a higher value (positive offset ΔE_c) than the conduction band minimum of the p-type absorber ,whereas the opposite occurs for the corresponding valence band maxima as it is shown in Figure 1. Theoretical calculations for CIGS/window heterostructures show that a slightly positive spike between 0.0-0.5 eV prevents losses in open circuit voltage (V_{oc}) due to a reduction of buffer/absorber interface recombination. Furthermore, this small spike has no negative influence on electron transport as theoretical calculation shows assuming thermionic emission across the junction.[3–5] In contrast, a too high spike in the conduction band will act as barrier for electrons, and therefore drastically reduce short circuit current (J_{sc}). The absence of a spike, i.e. a negative conduction band offset, called cliff (see Figure 1), leads to a drastically reduction of V_{oc} due to a reduction of the interface bandgap.[3]

Up to now highest efficiencies of 12.6% are reported for CZTSSe solar cells with CdS buffer layer grown by chemical bath deposition (CBD).[6] For CZTSSe absorber and CdS buffer positive conduction band offsets between 0.34 eV to 0.48 eV are reported, depending on the sulphur to selenium ratio (bandgap of absorber) and CdS deposition methods.[7,8] Due to the high toxicity of cadmium and the low band gap of CdS of 2.4 eV there is a high interest to replace this buffer layer with more environmental friendly material that is more transparent in the short-wavelength region of the visible solar spectrum to avoid absorption losses.

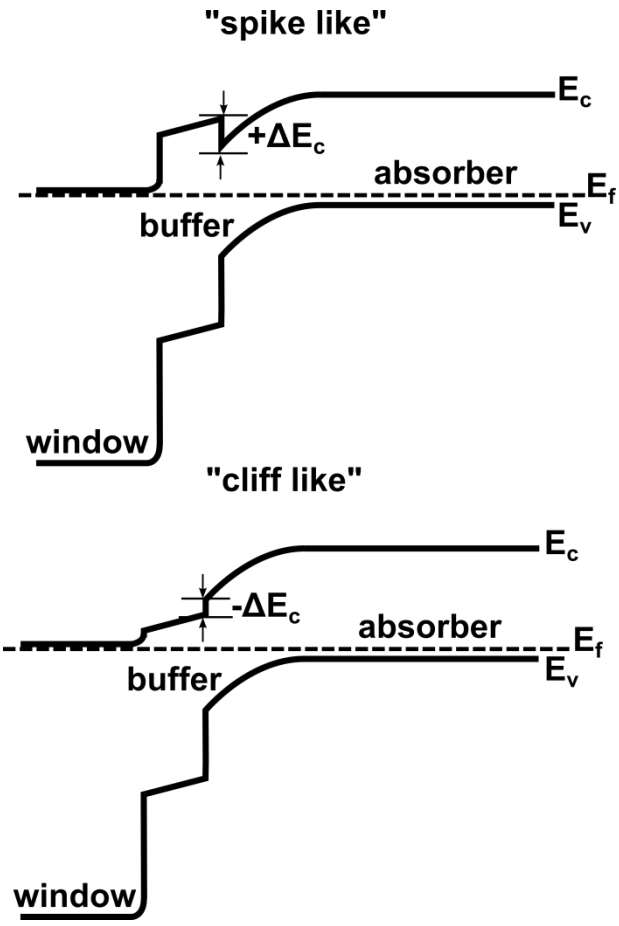

Figure 1. Schematics of the band diagrams of window/buffer/absorber heterostructures for spike and cliff like conduction band alignments.

ZnS(O,OH) is a promising alternative due to its low toxicity, higher bandgap and furthermore, the possibility to tune the band alignment depending on the sulphur to oxygen ratio.[9] Additionally, this material has demonstrated very encouraging results as buffer layer in CIGS technology, suggesting a good potentiality for being applied in kesterite based solar cells.[10] For CZTSSe ([S]/([S]+[Se]) = 0.4, E_g = 1.2 eV) and ZnS deposited by chemical bath deposition (CBD) a high spike like conduction band offset of 1.1 eV is reported.[11] For the same CZTSSe absorber and ZnO deposited by atomic layer deposition (ALD) a slightly cliff like offset is observed.[11] Devices prepared with this buffer layer show no (0.0%) and 2.46% efficiencies for , ZnS and ZnO respectively, whereas the CdS reference device yield 7.75% power conversion efficiency.[11] In Figure 2 the approximated band alignment of ZnS and ZnO with pure selenide CZTSe (E_g=1.0 eV) absorber is shown. A high spike and cliff like

alignment is expected for ZnS and ZnO, respectively. Thus, optimal band alignment necessary for high device performance could be adjusted by changing the ratio of oxygen to sulphur. For pure sulphide CZTS Ericson et al.[12] showed that the sulphur ratios in ALD deposited Zn(O,S) buffer layer have large influences on solar cell device performance resulting in devices with 4.6% efficiency for an optimized composition compared to 7.3% for reference CZTS/CdS device. Nguyen et al.[13] showed that thin 10-25nm ZnS buffer layer grown by CBD for monograin CZTSSe ([S]/([S]+[Se]) = 0.8) solar cells yield efficiencies up to 4.5% compared to a 4.8% CdS reference cell. Grenet et al.[14] report power conversion efficiency of 5.8% for CZTSSe ([S]/([S]+[Se]) = 0.15) devices with ZnS(O,OH) buffer deposited by CBD compared to 7.0% for CdS buffer device. However, a 24 hours light soaking was necessary to increase the power conversion efficiency from almost zero to a higher value due to metastabilities. In CIGS/ZnS(O,OH) based devices metastabilities are commonly observed and strongly depend on the absorber surface composition.[15] In CIGS it is reported that they can be reduced by increasing the buffer layer thickness, the use of a high resistive subsequently deposited i-ZnO layer or heat and light soaking treatments.[15,16]

In this study we present for the first time a variation of the thiourea (TU) concentration, i.e. the sulphur source, in the chemical bath of CBD grown ZnS(O,OH) buffer layer and its strong influence on device performances and stability of pure selenide CZTSe/ZnS(O,OH)/i-ZnO/ZnO:Al heterostructure solar cells.

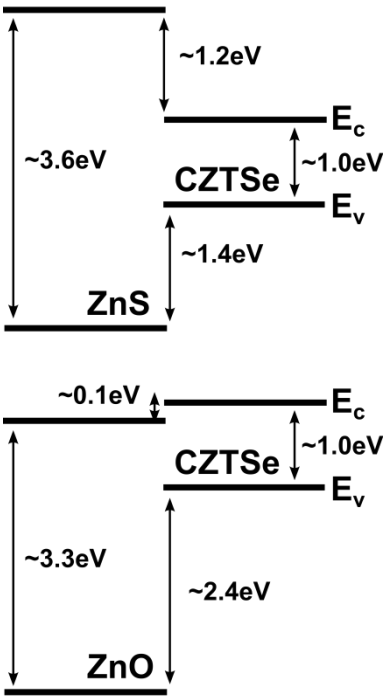

Figure 2. Approximation of band alignment of CZTSe absorber with ZnS (=" spike like") and ZnO (="cliff like"). Band offsets were taken from Barkhouse et al. [11] and adjusted to CZTSe absorber by shifting the valence band minimum according theoretical calculations.[17] A small spike like conduction band alignment (ΔE_c<0.5eV) would be preferable, which could be achieved by tailoring the S/O ratio in Zn(O,S)[9].

2. Experimental methods

Absorber synthesis. CZTSe absorbers were synthesized by a two stage approach. First Cu/Sn/Cu/Zn metal stacks were sputtered onto Mo coated soda lime glass followed by a reactive annealing in a graphite box under selenium and tin atmosphere as described elsewhere in more detail.[18,19] The synthesized absorber was split into equal pieces to investigate different buffer layers.

Buffer layer deposition. Prior to the buffer layer deposition, the absorbers were etched using KCN (10%wt.) for 30 seconds for surface cleaning. The ZnS(O,OH) buffer layers were grown by chemical bath deposition (CBD) using a $ZnSO_4$ (0.15 M)/ammonia (4.9 M)/thiourea aqueous solution. The CBD process is adapted from recipes reported in literature for high efficiency chalcopyrite/ZnS(O,OH) heterostructure solar cells.[16,20,21] The ammonia acts as complexing agent for the Zn^{+2} cations and thiourea is used as sulphur source. Four different

thiourea (TU) concentrations were investigated, namely 0.50 M, 0.40M, 0.35 M, and 0.30 M. The bath temperature was kept at 85ºC and the total duration for each of the runs was kept constant at 12 minutes for all samples. The CBD process can be described by following three simplified reaction equations

$$Zn(NH_3)_x^{2+} + S^{2-} \rightleftharpoons ZnS \downarrow + NH_3 \uparrow (1)$$

$$Zn(NH_3)_x^{2+} + 2OH^- \rightleftharpoons ZnO \downarrow + H_2O + NH_3 \uparrow (2)$$

$$Zn(NH_3)_x^{2+} + 2OH^- \rightleftharpoons Zn(OH)_2 \downarrow + NH_3 \uparrow (3)$$

Reaction (2) and (3) are competing due to their similar solubility product, whereas the one of ZnS (reaction (1)) is higher.[22] Reducing the sulphur concentration, i.e. thiourea (TU) concentration in the bath led to a decreased growth of ZnS. Reaction (2) and (3) are not affected thus an increased oxygen content in the final ZnS(O,OH) films can be expected. Immediately after the CBD process, samples were rinsed with 1.5 M ammonia aqueous solution and air annealed for 10 minutes at 200ºC as it was found beneficial for device performance.[23] Furthermore a reference cell with a standard CdS buffer layer was grown as well. Solar cells were completed with an i-ZnO/ZnO:Al bilayer (80nm/600nm) sputtered by RF magnetron sputtering. Individual cells with an area of 3x3 mm^2 were defined by mechanical scribing.

JV curves and external quantum efficiency (EQE). Solar cells were characterized by JV curves under 100 mW/cm^2 simulated AM1.5 solar illumination calibrated with a Si reference cell.

EQE was measured using a lock-in amplifier and a chopped white light source (900 W, halogen lamp, 360 Hz) combined with a dual grating monochromator which was calibrated using a Si reference cell.

Temperature dependent JV curves were recorded using a closed cycle He cryostat and a Oriel small area solar simulator calibrated to 1 sun with a Si reference cell.

Raman. ZnS(O,OH) layers were characterized by resonant Raman spectroscopy using a Horiba Jovin Yvon LabRam HR 800 –UV system coupled to a Olympus metallurgical microscope under 325 nm excitation wavelength, scanned over an area of 30 × 30 μm^2 using a DuoScan accessory. In order to avoid thermal effect the power density has been keep below to 0.4 mW in a spot of about 1 μm in diameter. All spectra were calibrated imposing the main peak of monocrystalline Silicon at 520 cm^{-1}.

X-ray photoelectron spectroscopy (XPS). XPS experiments were performed in a PHI 5500 Multitechnique System (from Physical Electronics) with a monochromatic X-ray source (Aluminium Kα line of 1486.6 eV energy and 350 W), placed perpendicular to the analyser axis and calibrated using the 3d5/2 line of Ag with a full width at half maximum (FWHM) of 0.8 eV.

3. Results and discussion

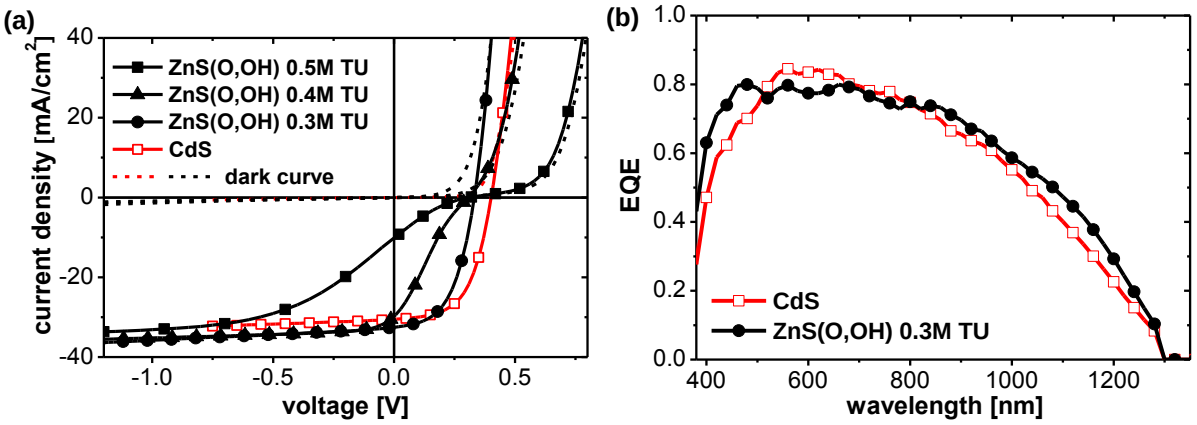

Figure 3. (a) Illuminated and dark JV curves of devices with ZnS(O,OH) buffer layer deposited with different thiourea (TU) concentrations during the CBD process and CdS as reference buffer layer. (b) External quantum efficiency of device with 0.3 M TU ZnS(O,OH) buffer and CdS buffer.

Figure 3 shows illuminated and dark JV curves of CZTSe absorbers with CdS reference and ZnS(O,OH) buffer layer deposited using three different thiourea (TU) concentrations in the bath. It can clearly be seen that for the sample with the highest TU concentration during CBD (0.50 M TU) the photocurrent (i.e. difference of current values of dark and illuminated JV curves) is starting to get blocked already at a reverse bias of -1.0 V. Then the JV curve shows

a kink like shape and follows the dark JV curve in forward bias direction. The solar cell device shows low efficiency with poor J_{sc} and FF (see Table 1). This behaviour is expected for a solar cell with a conduction band alignment showing a too high spike, since a too high spike acts as a barrier for photo generated electrons like a second diode. For the sample with ZnS(O,OH) 0.40 M TU concentration this current blocking occurs at a higher voltage and the distortion of the illuminated JV curve is less pronounced, indicating a reduction of the still too high barrier in the conduction band. This suggests less incorporation of sulphur into the ZnS(O,OH) film during the CBD process as discussed in the experimental section. However, the current blocking still starts at negative voltage (-0.1 V), which explains the lower J_{sc} value and FF obtained in comparison to the 0.30 M sample. For the sample ZnS(O,OH) 0.30 M TU no current blocking, i.e. distortion of the curve is observed. Comparing the device parameters of ZnS(O,OH) 0.30 M samples with the CdS reference cell (see Table 1) one can clearly see that the J_{sc} is around 2 mA/cm^2 higher, however the V_{oc} is still lower (332 mV compared to 401 mV, for ZnS(O,OH) 0.30 M and CdS respectively).

Table 1. Performance of devices with ZnS(O,OH) buffer layer deposited with different thiourea (TU) concentrations in the CBD process and CdS reference. R_{series}, R_{shunt} and ideality factor A were extracted from illuminated JV curves using the method described by Sites et al.[17]

buffer	CdS	ZnS(O,OH) 0.3M TU	ZnS(O,OH) 0.4M TU	ZnS(O,OH) 0.5M TU
Efficiency[%]	6.9	5.6	2.1	0.6
FF [%]	56.3	51.8	22.9	17.9
J_{sc} [mA/cm^2]	30.5	32.6	30.5	10.1
V_{oc} [mV]	401	332	306	311
R_{series} [Ω.cm^2]	0.85	0.72	-	-
R_{shunt} [Ω.cm^2]	235	131	-	-
A	2.14	2.02	-	-

The J_{sc} increase is expected because ZnS(O,OH) has a higher band gap than CdS, which increases its transparency, i.e. increases the absorption of short wavelength photons in the CZTSe absorber. EQE measurements, as shown in Figure 2 (b), confirm an increased charge carrier generation in the short wavelengths region below 500 nm. The lost in V_{oc} for the ZnS(O,OH) 0.30 M TU sample can be explained by a lower sulphur content in the buffer

layer and therefore a transition of a spike like alignment to a cliff, as it is also observed for CIGS with ALD deposited Zn(O,S) buffer layer with low sulphur content.[9] A very low sulphur content in the ZnS(O,OH) 0.30 M TU buffer layer of a value S/(S+O) < 0.04 was confirmed by Raman measurement, as will be discussed later. Therefore, a cliff like conduction band alignment as it is the case for pure ZnO (see Figure 2) is reasonable to assume. For both devices, CdS reference and ZnS(O,OH) 0.30 M TU, the diode ideality factor A is around 2 suggesting the main recombination paths limiting V_{oc} are trap states in the space charge region or the interface.[24] To determine if V_{oc} limitations are due to interface recombination temperature dependent JV curves were recorded. In Figure 3 the temperature dependence of the V_{oc} for the ZnS(O,OH) 0.30 M TU and CdS reference device is shown. From a linear extrapolation of the V_{oc} to 0K the activation energy of recombination can be calculated ($E_a=V_{oc}*q$; q…elementary charge). A clear difference between ZnS(O,OH) 0.30 M TU and CdS reference can be seen. For CdS reference an activation energy of E_a=0.88 eV was extracted which is close to the fundamental bandgap of CZTSe of 1.0 eV. For ZnS(O,OH) 0.30 M TU the activation energy is clearly lower, at a value of 0.48 eV. Thus, an increased interface recombination due to the presence of a cliff like conduction band alignment reduces the V_{oc} of 0.30 M TU device as discussed earlier.

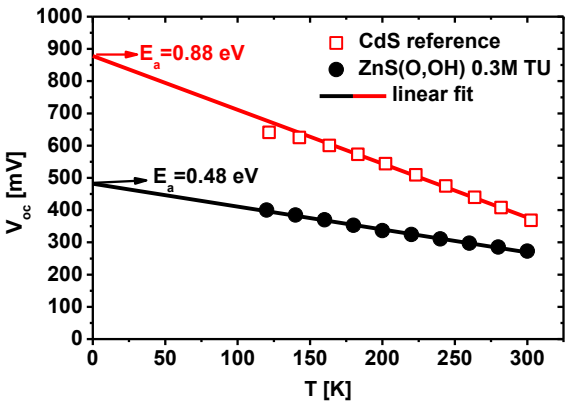

Figure 4. Temperature dependence of V_{oc} and linear extrapolation to T=0K to etract the activation energy of the recombination process for solar cells with ZnS(O,OH) 0.3 M TU and CdS buffer layers.

Although, from a first sight the efficiency of ZnS(O,OH) 0.30 M TU sample seems better than for the 0.40 M TU sample, a cliff like band alignment is a clear limitation for device performance. As will be shown in the following, light soaking treatments can largely improve performance of devices with ZnS(O,OH) buffer layers with higher sulfur content, i.e. spike like band alignment.

To characterize the ZnS(O,OH) layers grown onto CZTSe absorber and proof the reproducibility of the process a new set of samples was prepared using four different TU concentrations (0.30 M, 0.35M, 0.40 M, and 0.50 M). One part of each sample was completed to solar cells and one was kept for characterization of the buffer layer itself.

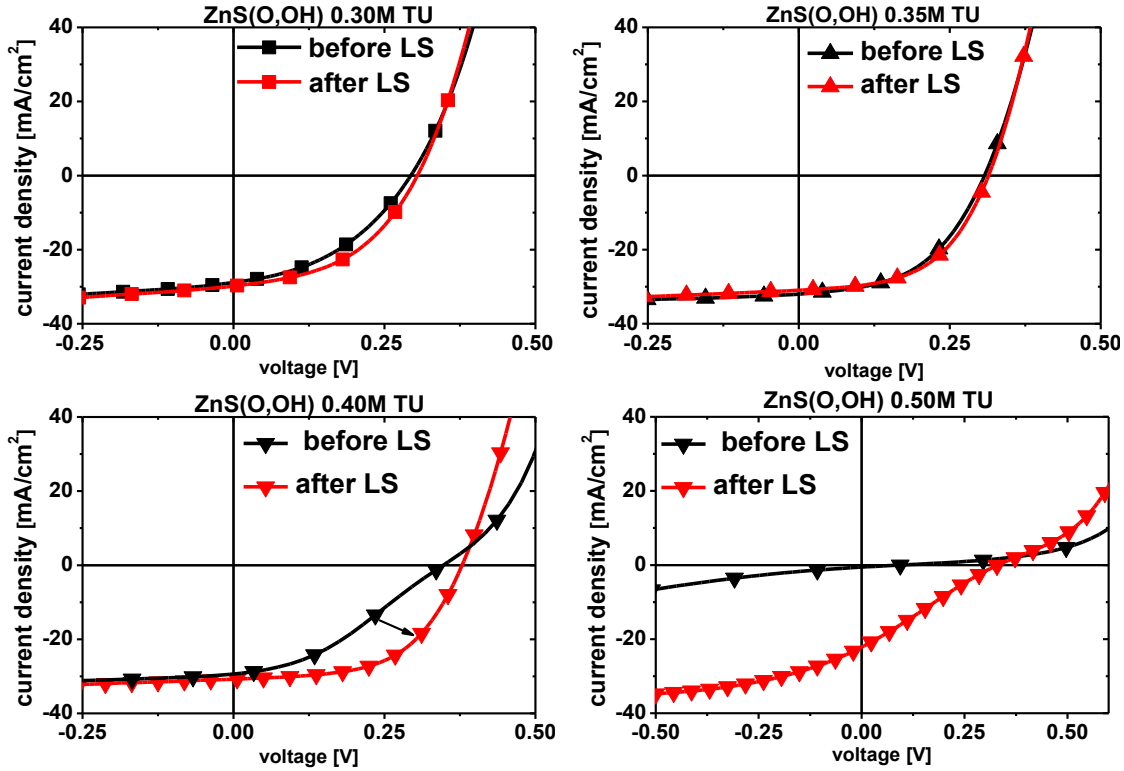

Figure 5. Illuminated JV curves of devices with ZnS(O,OH) buffer layer deposited with different thiourea (TU) concentrations during the CBD process before and after light soaking for 260 minutes.

Table 2. Performance of devices with ZnS(O,OH) buffer layer deposited with different thiourea (TU) concentrations during the CBD process before and after light soaking (LS) for 260 minutes. R_{series}, R_{shunt} and ideality factor A were extracted from illuminated JV curves using the method described by Sites et al.[25]

buffer	ZnS(O,OH) 0.30M TU		ZnS(O,OH) 0.35M TU		ZnS(O,OH) 0.40M TU		ZnS(O,OH) 0.50M TU	
	before	after LS	before	after LS	before	after LS	before	after LS
Efficiency[%]	3.5	4.2	4.8	5.1	3.6	6.5	0.01	1.8
FF [%]	41.1	45.7	49.2	52.5	35.3	55.9	24.1	24.7
J_{sc} [mA/cm^2]	28.9	29.8	32.0	30.9	29.4	30.7	0.6	22.2
V_{oc} [mV]	294	304	308	311	348	379	96	330
R_{series} [Ω.cm^2]	0.38	0.50	0.64	0.55	-	0.55	-	-
R_{shunt} [Ω.cm^2]	48	59	97	114	143	174	-	-
A	3.3	2.6	2.3	2.1	-	2.1	-	-

In Figure 5 JV curves of these devices are shown and its device parameters summarized in Table 2. All devices show same behaviour as for the first set of sample, with non-distorted curves for low TU deposited buffer and kinks for 0.40 M and 0.50 M samples. Furthermore, for this set of samples the effects of light soaking (LS) were studied in detail. Since, all CZTSe absorber layer used were produced in the same synthesis run all observed differences in light soaking behaviour can be attributed to the properties of the different ZnS(O,OH) buffer layers. In Figure 6 the evolution of device parameters depending on one sun white light soaking time are presented and the device parameters before and after LS are summarized in Table 2. It can clearly be seen that 0.30 M and 0.35 M sample are almost not affected by LS. However, LS has a large influence on the 0.40 M and 0.50 M sample. Already after the first 10 minutes of LS a large increase in device performance is observed for the 0.40 M sample from 3.5 % to 5.8% efficiency which further stabilizes at 6.5% after 250 minutes. Comparing the JV-curves before and after LS in Figure 5 one can see that LS eliminates the JV curve distortion, leading to a strong increase in V_{oc}, J_{sc}, and FF. Also for the 0.50 M device a strong improvement in device performance is observed. With increasing LS time JV distortion is reduced allowing collection of photo-generated charge carriers. This indicates a reduction of the barrier present for photo generated electrons, i.e. reduction of the spike in the conduction band due to photo doping of the ZnS(O,OH).[26] The beneficial effect of LS can be explained by the presence of acceptor like deep states in the buffer layer, buffer/absorber or

buffer/window interface as widely reported in literature.[26–28] In dark or after only short illumination these acceptors like states are ionized by trapping electrons contributed by the donors of the n-type buffer layer, thus compensating it. A more negative space charge is created inside the buffer layer which results in a decrease in band bending and increase of the conduction band spike as illustrated in Figure 7. During white light illumination photo generated holes in the buffer layer get trapped by the acceptor defects, i.e. neutralizing them and reducing the spike again (see Figure 7). This is due to the fact that negatively charged acceptor like defects have larger capture crosssection for holes than when they are neutral for electrons.[26] Since during illumination electron hole pairs are created inside of the buffer a large amount of free holes is present which can be captured and neutralize the defect. Therefore, white light soaking (LS) can reduce the conduction band spike slightly. Thus the low influence of LS and lower V_{oc} of the 0.30 M and 0.35 M devices further suggests a cliff like conduction band alignment in contrast to the 0.40 M and 0.50 M devices.[29] After 150 minutes LS the V_{oc} of the 0.50 M device even overcomes the ones of the 0.30 M and 0.35 M devices.

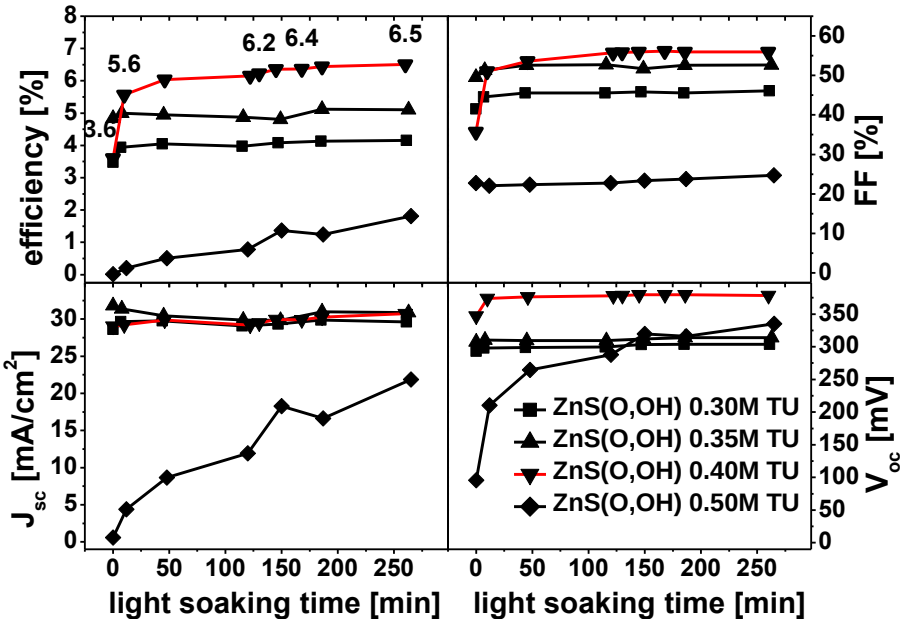

Figure 6. Evolution of device parameters with 1 sun light soaking time for devices with ZnS(O,OH) buffer layer deposited with different thiourea (TU) concentrations during the CBD process.

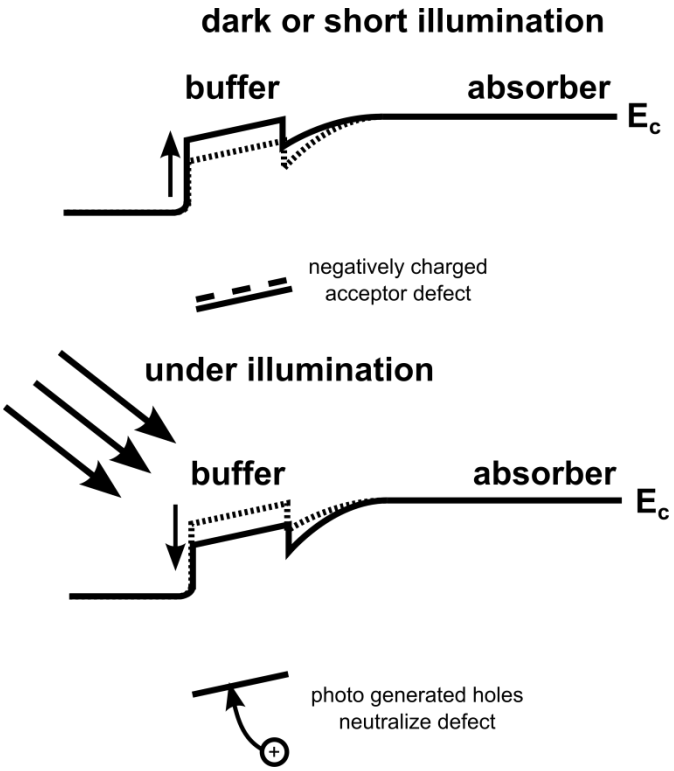

Figure 7. Schematic of the conduction band alignment in the presence of acceptor like deep defect states. In dark these defects are negatively charged due to trapping of electrons contributed from the donors of the buffer layer. This negative space charge decreases the band bending and increases the spike in the conduction band. Under illumination photogenerated holes can neutralize the defects resulting in a decrease of the spike.

To characterize the ZnS(O,OH) layers itself, XPS measurements were carried out on sister pieces of the Mo/CZTSe/ZnS(O,OH) layers that were finished to solar cells (see Figure 8 (a)). XPS shows that all four ZnS(O,OH) layers are below 10 nm with estimated thicknesses of below 2 nm for the 0.30 M and 0.35 M case, 6 nm for 0.40 M and around 9 nm for the 0.50 M case, calculated by using multipack fit program and the NIST database for the estimation of the electron inelastic mean free path. For the 0.30 M and 0.35 M case even the Cu and Se peaks of the CZTSe layer beneath are visible confirming a thickness of around 2 nm. Full coverage of all layers is assumed, since no sever shunting of devices is observed even after applying high reverse bias voltages (see Figure 3 and 5). Other direct or indirect thickness measurements of this nanometric buffer layers on top of absorbers are challenging since the CZTSe absorber surface is quite rough which makes the use of optical based measurements

impossible. The use of other smoother substrates would influence largely the growth conditions which could lead to misinterpretations when comparing to ZnS(O,OH) grown onto CZTSe absorbers. In general this fact and the low thickness make further advanced electrical, optical or compositional characterization of the exactly same buffer layers as used in solar cell devices a difficult task. To determine S/(S+O) ratios a carbon surface layer had to be removed by argon sputtering unfortunately leading to the removal of the full layer for 0.30 M, 0.35 M and 0.40 M samples due to their nanometric thickness. For 0.50 M sample an S/(S+O) ratio of 0.63 was calculated. The ZnS(O,OH) layers were further investigated by resonant Raman measurements which are very sensitive to bandgap modifications of materials originated from composition change or nanotexturization.[30–32] In the measured spectra a ZnO–like LO Raman peak was found for the 0.30 M sample and a ZnS-like LO Raman peak for the 0.50 M sample (see Figure 8 (b)). This fact indicates a different incorporation of sulphur and oxygen due to changes in the TU concentration during CBD as already suggested by the observed solar cell device performance. For the 0.30 M sample the frequency of the ZnO-like LO peak is very close to that from the measured pure ZnO reference. This indicates that this layer has a very low S content, with a value S/(S+O) < 0.04 according to the dependence of the frequency of this peak on the S/(S+O) content reported in A. Polity et al.[33] In the spectra from the 0.35 M and 0.40 M samples only CZTSe characteristic Raman peaks were observed.[34,35] This could be related with a loss of the resonant Raman excitation conditions when using the UV excitation line in these very thin layers because of the strong band gap bowing that takes place in Zn(O,S) alloys with S/(S+O) relative content close to 0.5.[33] In case of sample 0.50 M the ratio of first (at 347 cm^{-1}) and second (at 692 cm^{-1}) order ZnS like Raman peaks allows to make an estimation of the grain size in the layer of below 10 nm which is in agreement with the XPS estimated thickness below 9 nm.[30]

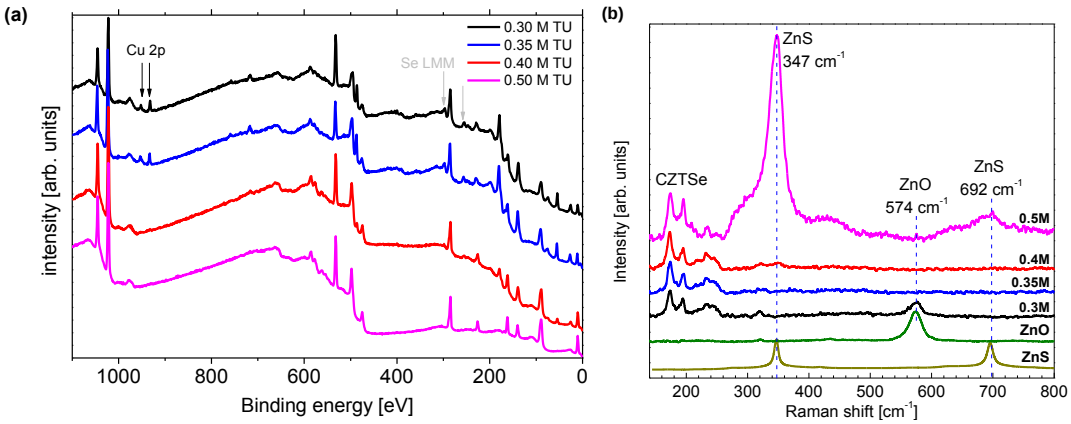

Figure 8. X-ray photoelectron spectroscopy (a) and UV-Raman (b) spectra and of ZnS(O,OH) buffer layer on CZTSe absorber deposited with different thiourea (TU) concentrations during the CBD process; ZnO and ZnS reference spectra were add for convenience.

4. Conclusion

In conclusion, this work shows that CBD grown ZnS(O,OH) buffer layers give promising results for cadmium free CZTSe based solar cells with power conversion efficiencies of up to 6.5% after light soaking, a value comparable to that of the CdS reference case. Variation of the thiourea concentration in the CBD shows strong impact on device performance. A strong distortion (kink) in illuminated JV curves is observed for high TU concentration samples (0.5-0.4 M) indicating a barrier for photo-generated electrons as expected for ZnS as buffer layer due to a too high spike like conduction band alignment.[11] No distortions, however, lower V_{oc} values are obtained for 0.35 and 0.30 M TU devices. Furthermore, 0.35 M and 0.30 M samples are less affected by light soaking, whereas, 0.40 M and 0.50 M devices show strong improvements after light soaking. XPS and Raman indicate layer thicknesses of less than 10 nm for all cases, and a decrease in thickness with decreasing TU concentration. Variations of S/(S+O) ratios are not evident from XPS due to carbon surface contamination and the low layer thickness. However, Raman scattering spectra exhibited ZnO-like peak for 0.30 M sample and ZnS-like peaks for 0.50 M sample. The observed decrease of thickness with decreasing TU concentration together with a strong reduction of metastable behaviour is another indication for changes in S/(S+O) ratio, i.e. band alignment, since in CIGS the

opposite thickness related trend is observed.[15] However, for CIGS it is shown that metastable effects can be reduced by reducing the conduction band offset towards a cliff.[29] On the whole, getting insights in the strong influence of thiourea concentration in CBD of ZnS(O,OH) buffer layers on device performance opens up new easy ways to further increase efficiencies of environmental friendly cadmium free earth abundant solar cells.

Acknowledgements

This research was supported by the Framework 7 program under the project KESTCELLS (FP7-PEOPLE-2012-ITN-316488), by the NOVAZOLAR project from the SOLARERANET International program (subproject ref. PCIN-2013-193 funded by Spanish MINECO) and by European Regional Development Founds (ERDF, FEDER Programa Competitivitat de Catalunya 2007–2013). Authors from IREC and the University of Barcelona belong to the M-2E (Electronic Materials for Energy) Consolidated Research Group and the XaRMAE Network of Excellence on Materials for Energy of the "Generalitat de Catalunya". E.S. thanks the Government of Spain for the "Ramon y Cajal" fellowship (RYC-2011-09212) and Y.S. thanks for the PTA fellowship (PTA2012-7852-A).

References

[1] A. Polizzotti, I. L. Repins, R. Noufi, S.-H. Wei, D. B. Mitzi, *Energy Environ. Sci.* **2013**, DOI 10.1039/c3ee41781f.
[2] R. Scheer, H. W. Schock, Wiley InterScience (Online service), *Chalcogenide Photovoltaics Physics, Technologies, and Thin Film Devices*, Wiley-VCH ; John Wiley [distributor], Weinheim; Chichester, **2011**.
[3] T. Minemoto, T. Matsui, H. Takakura, Y. Hamakawa, T. Negami, Y. Hashimoto, T. Uenoyama, M. Kitagawa, *Sol. Energy Mater. Sol. Cells* **2001**, *67*, 83.
[4] M. Gloeckler, J. R. Sites, *Thin Solid Films* **2005**, *480–481*, 241.
[5] A. Niemegeers, M. Burgelman, A. D. Vos, *Appl. Phys. Lett.* **1995**, *67*, 843.
[6] W. Wang, M. T. Winkler, O. Gunawan, T. Gokmen, T. K. Todorov, Y. Zhu, D. B. Mitzi, *Adv. Energy Mater.* **2013**, 4, 1301465
[7] R. Haight, A. Barkhouse, O. Gunawan, B. Shin, M. Copel, M. Hopstaken, D. B. Mitzi, *Appl. Phys. Lett.* **2011**, *98*, 253502.
[8] J. Li, M. Wei, Q. Du, W. Liu, G. Jiang, C. Zhu, *Surf. Interface Anal.* **2013**, *45*, 682.
[9] C. Platzer-Björkman, T. Törndahl, D. Abou-Ras, J. Malmström, J. Kessler, L. Stolt, *J. Appl. Phys.* **2006**, *100*, 044506.
[10] M. Nakamura, N. Yoneyama, K. Horiguchi, Y. Iwata, K. Yamaguchi, H. Sugimoto, T. Kato, in *Photovolt. Spec. Conf. PVSC 2014 IEEE 40th*, IEEE, **2014**, pp. 0107–0110.

[11] D. A. R. Barkhouse, R. Haight, N. Sakai, H. Hiroi, H. Sugimoto, D. B. Mitzi, *Appl. Phys. Lett.* **2012**, *100*, 193904.
[12] T. Ericson, J. J. Scragg, A. Hultqvist, J. T. Watjen, P. Szaniawski, T. Torndahl, C. Platzer-Bjorkman, *IEEE J. Photovolt.* **2014**, *4*, 465.
[13] M. Nguyen, K. Ernits, K. F. Tai, C. F. Ng, S. S. Pramana, W. A. Sasangka, S. K. Batabyal, T. Holopainen, D. Meissner, A. Neisser, L. H.Wong, *Sol. Energy* **2015**, *111*, 344.
[14] L. Grenet, P. Grondin, K. Coumert, N. Karst, F. Emieux, F. Roux, R. Fillon, G. Altamura, H. Fournier, P. Faucherand, S. Perraud, *Thin Solid Films* **2014**, DOI 10.1016/j.tsf.2014.05.033.
[15] M. Buffière, N. Barreau, L. Arzel, P. Zabierowski, J. Kessler, *Prog. Photovolt. Res. Appl.* **2014**, DOI: 10.1002/pip.2451.
[16] T. Kobayashi, H. Yamaguchi, T. Nakada, *Prog. Photovolt. Res. Appl.* **2014**, *22*, 115.
[17] A. Walsh, S. Chen, S.-H. Wei, X.-G. Gong, *Adv. Energy Mater.* **2012**, *2*, 400.
[18] S. López-Marino, M. Placidi, A. Pérez-Tomás, J. Llobet, V. Izquierdo-Roca, X. Fontané, A. Fairbrother, M. Espíndola-Rodríguez, D. Sylla, A. Pérez-Rodríguez, E. Saucedo, *J. Mater. Chem. A* **2013**, *1*, 8338.
[19] M. Neuschitzer, Y. Sanchez, S. López-Marino, H. Xie, A. Fairbrother, M. Placidi, S. Haass, V. Izquierdo-Roca, A. Perez-Rodriguez, E. Saucedo, *Prog. Photovolt. Res. Appl.* **2015**, DOI: 10.1002/pip.2589.
[20] A. Ennaoui, M. Bär, J. Klaer, T. Kropp, R. Sáez-Araoz, M. C. Lux-Steiner, *Prog. Photovolt. Res. Appl.* **2006**, *14*, 499.
[21] T. Nakada, M. Mizutani, Y. Hagiwara, A. Kunioka, *Sol. Energy Mater. Sol. Cells* **2001**, *67*, 260.
[22] C. Hubert, N. Naghavi, B. Canava, A. Etcheberry, D. Lincot, *Thin Solid Films* **2007**, *515*, 6032.
[23] M. Neuschitzer, Y. Sanchez, T. Olar, T. Thersleff, S. Lopez-Marino, F. Oliva, M. Espindola-Rodriguez, H. Xie, M. Placidi, V. Izquierdo-Roca, I. Lauermann, K. Leifer, A. Pérez-Rodriguez, E. Saucedo, *Chem. Mater.* **2015**, 27 (15), 5279–5287.
[24] S. S. Hegedus, W. N. Shafarman, *Prog. Photovolt. Res. Appl.* **2004**, *12*, 155.
[25] J. R. Sites, P. H. Mauk, *Sol. Cells* **1989**, *27*, 411.
[26] I. . Eisgruber, J. . Granata, J. . Sites, J. Hou, J. Kessler, *Sol. Energy Mater. Sol. Cells* **1998**, *53*, 367.
[27] A. O. Pudov, J. R. Sites, M. A. Contreras, T. Nakada, H.-W. Schock, *Thin Solid Films* **2005**, *480-481*, 273.
[28] M. Nichterwitz, R. Caballero, C. A. Kaufmann, H.-W. Schock, T. Unold, *J. Appl. Phys.* **2013**, *113*, 044515.
[29] H. Hori, T. Minemoto, H. Takakura, *Curr. Appl. Phys.* **2010**, *10*, S150.
[30] A. Fairbrother, V. Izquierdo-Roca, X. Fontané, M. Ibáñez, A. Cabot, E. Saucedo, A. Pérez-Rodríguez, *CrystEngComm* **2014**, *16*, 4120.
[31] M. Dimitrievska, H. Xie, A. Fairbrother, X. Fontané, G. Gurieva, E. Saucedo, A. Pérez-Rodríguez, S. Schorr, V. Izquierdo-Roca, *Appl. Phys. Lett.* **2014**, *105*, 031913.
[32] V. Izquierdo-Roca, X. Fontané, E. Saucedo, J. S. Jaime-Ferrer, J. Álvarez-García, A. Pérez-Rodríguez, V. Bermudez, J. R. Morante, *New J Chem* **2011**, *35*, 453.
[33] A. Polity, B. K. Meyer, T. Krämer, C. Wang, U. Haboeck, A. Hoffmann, *Phys. Status Solidi A* **2006**, *203*, 2867.
[34] M. Guc, S. Levcenko, V. Izquierdo-Roca, X. Fontane, M. Y. Valakh, E. Arushanov, A. Pérez-Rodríguez, *J. Appl. Phys.* **2013**, *114*, 173507.
[35] M. Dimitrievska, A. Fairbrother, E. Saucedo, A. Pérez-Rodríguez, V. Izquierdo-Roca, *Appl. Phys. Lett.* **2015**, *106*, 073903.